Optimal Coordinated Design of Under-Frequency Load Shedding and Energy Storage Systems

Paola Santurino, Lukas Sigrist, Álvaro Ortega, Javier Renedo, Enrique Lobato
IIT, ETSI ICAI
Universidad Pontificia Comillas, Madrid, Spain
lukas.sigrist@iit.comillas.edu

***Abstract*— Under-frequency load shedding (UFLS) is considered a fundamental protection tool against power imbalances in electrical grids, particularly in small island systems. However, load shedding entails a delicate compromise between guaranteeing the stability of the system and disconnecting the lowest amount of load to achieve it. Fast-responding converter-interfaced energy storage systems (ESSs) can help improve such a compromise. In this regard, this paper proposes a methodology for the coordinated design of under-frequency load shedding (UFLS) and fast-responding converter-interfaced energy storage systems (ESSs). UFLS parameters include thresholds for frequency and its rate-of-change, and time settings of each step. ESS control parameters comprise, among others, the emulated inertia and the droop. The proposed coordinated methodology is applied to a real Spanish island power system with a 4 MW/5.6 kWh ultracapacitor (UC). Results show that the proposed methodology is able to significantly reduce the total amount of load shed with respect to the currently implemented UFLS settings and UC control parameters.**

***Index Terms*—Frequency stability, under-frequency load shedding, energy storage systems, ultracapacitors, island grids**

I. INTRODUCTION

Under-frequency load shedding (UFLS) schemes play a fundamental role in the protection of a power system against power imbalances. Island power system are particularly sensitive to power imbalances [1], [2]. UFLS schemes continuously measure frequency and optionally the rate of change of frequency (RoCoF) by means of type 81 relays [3] and shed a predefined amount of load if frequency and/or RoCoF fall below a certain threshold. UFLS schemes thus entail a sensitive compromise between efficiency (i.e., shedding the lowest amount of load possible to maintain system stability), and robustness (i.e., ensuring system stability under different operating conditions).

The delicate equilibrium discussed above can be efficiently improved through fast-responding, converter-interfaced energy storage systems (ESSs) [4]. Several works in the literature discuss the joint operation of UFLS schemes and ESS frequency controllers. A study of an ESS with RoCoF-based control installed in a Malayan isolated microgrid to compensate active power imbalances, thus avoiding or minimizing load shedding, is presented in [5]. In [6], the ESS is operated such that it injects its rated power until the frequency value starts its restoration after reaching the frequency nadir. A model-predictive control is then applied to restore the load level while reducing the ESS power injection. An adaptive, three-stage UFLS scheme coordinated with an ESS is proposed in [7], whereas [8] presents a methodology for sizing an ESS to minimize the amount of load shed.

From [6], it is deduced that, for reducing the load shedding actions, it will suffice with ESSs with low energy-to-power ratios, provided that their frequency control schemes are adequately designed. Among the converter-interfaced ESS technologies that fall into this category, ultracapacitors (UCs) are of particular relevance, given their level of maturity. UCs are characterized by high energy-conversion efficiencies and lifetime cycles, and remarkably fast response times. UCs are thus highly suitable to improve the frequency response of the grid (see, e.g., [9]), and thus, the efficiency of UFLS schemes. The impact of the limited energy capacity of the UC is studied in [10].

All references above prove that installing an ESS in island grids has a direct impact on the reduction of the UFLS actions. Nevertheless, integration of ESSs does not fully eliminate the need for such UFLS schemes. There is thus a necessary coupling between the ESS (and its control parameters), and the UFLS (and its relay settings). The design of robust and efficient UFLS schemes alone has been addressed in the literature [2]- [11]. Similar to [2], the UFLS scheme in [12] has been tuned by using Improved Harmony Search to minimize the total amount of shed. Reference [13] formulates a mixed-integer linear programming (MILP) problem to tune UFLS parameters including the step size, and finally selects the most appropriate scheme according to scoring method based on the frequency response quality. A stochastic MILP problem is applied in [11], considering load and renewable energy resource uncertainties. However, to the best of our knowledge, no study has yet focused on the benefits of simultaneously tuning ESS and UFLS control/relay parameters.

This paper fills this gap, and proposes a methodology to determine the optimal control and relay parameters of an ESS and an UFLS scheme for a coordinated response against under-frequency events in island systems. The optimization algorithm is formulated with the aim to find the best compromise between robustness and efficiency. The objective of the proposed methodology is the minimization of the UFLS actions while maximizing the ESS contribution. The paper

Submitted to the 22nd Power Systems Computation Conference (PSCC 2022).

does not tackle the sizing of the ESS since this would also require considering aspects related to the techno-economic operation of small island power systems.

The remainder of the paper is organized as follows. Section II provides the modeling framework of an island system with a UFLS scheme and an ESS for frequency stability analysis. The proposed coordinated design method for the UFLS and ESS is presented in Section III. Section IV discusses the case study, which is based on a real-world island system in Spain with inclusion of a UC and a UFLS scheme. Finally, Section V draws conclusions and outlines future work directions.

II. SYSTEM MODEL

This section presents the models considered in this paper to represent the dynamic behavior of an island system with UFLS scheme and an ESS. The model of the overall system is discussed in Section II-A, whereas the ESS model is presented in Section II-B.

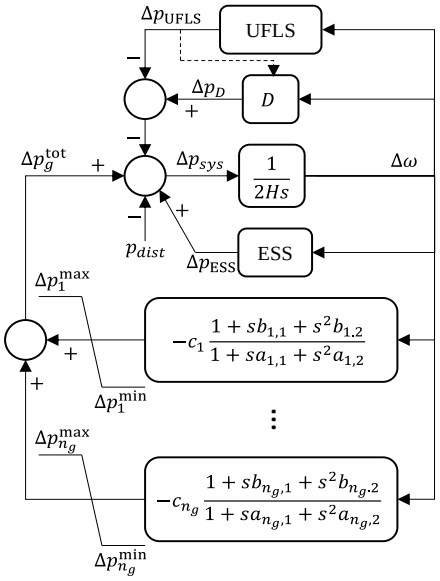

Figure 1. Simplified model of an island system.

A. Island System Model with UFLS Scheme

Figure 1 depicts the scheme of the simplified model representing the dynamic behavior of an island system with n_g synchronous generators, UFLS scheme and an ESS [2]. Active power imbalances are modeled with the term p_{dist}.

Each synchronous generator uses a second-order transfer function that approximates the response of the turbine and speed governor. It is thus assumed that generator subtransient and excitation system dynamics can be neglected for the frequency stability analysis discussed in this paper. Parameters c_i, $a_{i,j}$ and $b_{i,j}$ of each generator can be estimated from more detailed models, or from field-test measurements. Generator power limits, $\Delta p_i^{\min}$ and $\Delta p_i^{\max}$, are also modeled.

In the model shown in Figure 1, the network has also been neglected. Therefore, all generators and loads are connected to a single bus. This leads to the assumption of a unique system frequency that varies uniformly across the network. This assumption is well justified for island systems with relatively short transmission and distribution lines. In such systems, local frequency oscillations are fairly small compared to the overall frequency trend, as shown in Figure 2, where frequency variations due to a 3.5 MW generation outage with and without modeling the network are shown.

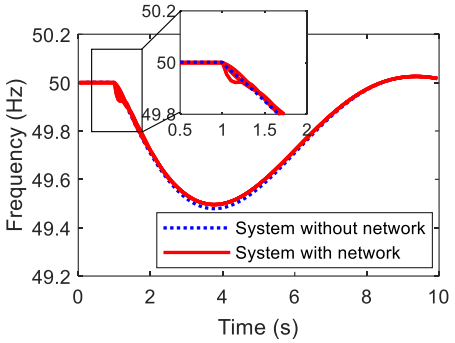

Figure 2. Response of a Spanish island power system in terms of frequency to a 3.5 MW generation outage with and without modeling the network.

The single-bus model of the network implies that, in p.u., an equivalent synchronous rotor can be characterized by an equivalent system inertia H that links frequency $(\Delta\omega)$ and active power (Δp_{sys}) variations.

Finally, it is assumed that the load power variations, ΔP_D, do not depend on local variations of the voltage magnitude, but on the frequency variations through the load damping factor, D. When the UFLS block activates, the demand consumption is reduced by an amount Δp_{UFLS}, according to the UFLS scheme settings. If the loads affected by the UFLS actions are frequency dependent, then the D needs to be adjusted according to:

$$D(t) = D_0 \left(\frac{P_D}{S_{base}} - \Delta p_{\text{UFLS}}(t) \right) \quad (1)$$

where D_0 is the demand initial damping factor; P_D is the initial demand active power consumption; and Δp_{UFLS} is the amount of load shed due to the perturbation. Since the load damping factor is usually unknown, typical values between 1 and 2% are assumed [14]. Here, the load damping factor has been neglected without loss of generality.

Figure 3 shows and compares frequency variations of the island power system described in section IV to generation outages of 2.35 MW (top panel) and 3.25 MW (bottom panel), respectively. These frequency variations have been simulated with the simplified model of Figure 1 and with a fully detailed power system model. The generation outage of 3.25 MW leads to UFLS, which can be observed in the abrupt changes in the frequency. In general, it can be seen that the simplified power system model accurately represents

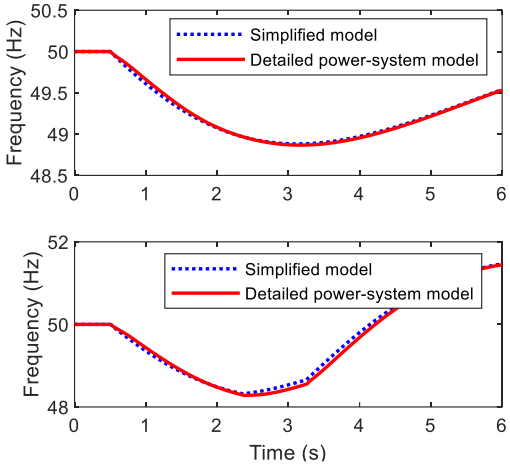

Figure 3. Comparison of the simulated response with the simplified and a detailed power system model. Top panel: 2.35 MW outage. Bottom panel: 3.25 MW outage.

B. ESS Model

Figure 4 illustrates the block diagram of the converter-interfaced ESS model used here for the frequency stability studies [15]. The model represents the behavior of the ESS, the fast-frequency controller (with droop and virtual inertia control), and the power converter that interfaces the storage device with the grid.

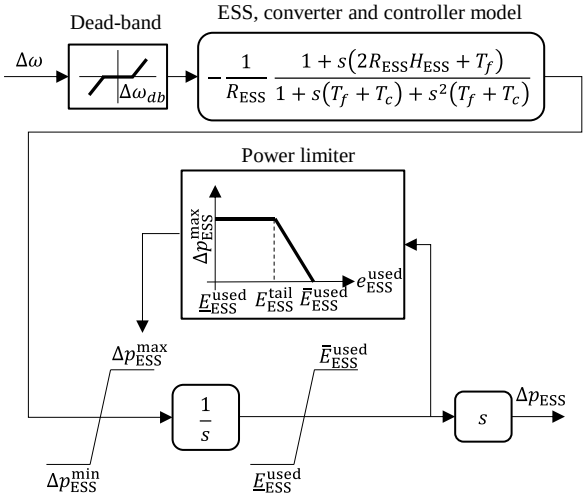

Figure 4. ESS model for frequency stability analysis.

The scheme depicted in Figure 4 includes a dead-band block to filter small-amplitude variations of the system frequency, $\Delta\omega_{db}$. The model of the ESS, power converter and fast-frequency controller is then jointly represented by a second-order transfer function where R_{ESS} and H_{ESS} are the droop and virtual inertia coefficients, respectively, whereas T_f and T_c are the time constants of the filter and of the equivalent inner- and outer-current controls of the converter, respectively.

The model also includes upper and lower limits for active power ($\Delta p_{\mathrm{ESS}}^{\min}$ and $\Delta p_{\mathrm{ESS}}^{\max}$) and energy used ($\underline{E}_{\mathrm{ESS}}^{\mathrm{used}}$ and $\bar{E}_{\mathrm{ESS}}^{\mathrm{used}}$) of the ESS. The energy used, $e_{\mathrm{ESS}}^{\mathrm{used}}$, is the opposite of the available stored energy. It is assumed that the ESS is initially fully charged, meaning that $\underline{E}_{\mathrm{ESS}}^{\mathrm{used}} = 0$. To prevent abrupt transients due to energy depletion of the ESS, a so-called *tail control* is also implemented, which gradually reduces the active power injection of the ESS when the ESS is getting depleted, i.e., when $e_{\mathrm{ESS}}^{\mathrm{used}}$ approaches $\bar{E}_{\mathrm{ESS}}^{\mathrm{used}}$. The proximity of $e_{\mathrm{ESS}}^{\mathrm{used}}$ to its upper limits is defined by the threshold $E_{\mathrm{ESS}}^{\mathrm{tail}}$, which represents a percentage of the usable energy of the ESS, $\left(\bar{E}_{\mathrm{ESS}}^{\mathrm{used}} - \underline{E}_{\mathrm{ESS}}^{\mathrm{used}}\right)$. Indeed, the tail control acts like an anti-wind up, bringing the power to zero when $\bar{E}_{\mathrm{ESS}}^{\mathrm{used}}$ is reached. The ESS can also absorb power during the frequency transients (e.g., when frequency is shortly above the nominal frequency).

III. DESIGN OF OPTIMAL COORDINATED CONTROL OF UFLS AND ESS

The methodology to design the optimal coordinated control of the UFLS scheme and the ESS fast-frequency control in an island system proposed in this paper is described below. The clustering of scenarios based on the most representative responses is discussed in Section III-A. Section III-B formulates the optimization problem that defines the parameters of the UFLS and ESS. Finally, Section III-C outlines the implementation details involved in the practical application of the proposed methodology.

A. Most-representative Contingencies Definition – K-Means Scenario Clustering

Adjusting the UFLS and ESS parameters for each and every possible contingency, although robust, is not an efficient solution to be implemented in practice. A trade-off between robustness and efficiency needs thus to be achieved when designing the UFLS scheme and ESS control. This is possible if an adequate selection of the set of most-representative contingencies that can disturb the system is performed.

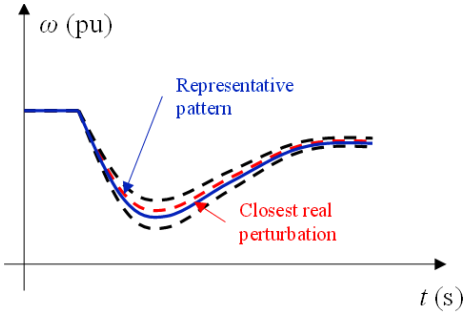

Figure 5. Illustration of scenario clustering.

To this aim, the K-means algorithm proposed in [2] is used in this paper to identify the most-representative contingencies. The K-means algorithm thus determines, based on the dynamic frequency responses of "all" possible contingencies, the patterns that best describe such responses. The scenario

clustering is graphically illustrated in Figure 5 for three trajectories and one representative pattern.

Note that, in the majority of cases, the patterns identified by the K-means algorithm will be fictitious, i.e., they will not correspond to an actual frequency response of the real system. Thus, a final step in the scenario clustering process involves the identification of the real response that best approximates the calculated patterns. Statistical analysis tools such as principal components can be then used to evaluate the quality of the selection of representative contingencies [16].

B. Optimization Algorithm of UFLS and ESS Coordinated Control

The process of identifying the parameters of the UFLS scheme and ESS control for a coordinated operation can be formulated as an optimization problem aimed at minimizing the total amount of load shed for all representative contingencies identified as described in Section III-A above while satisfying a set of constraints. Such constraints include upper and lower bounds for the system frequency variations, the amount of load shed, and the ESS response.

1) Objective Function and Decision Variables: The objective function of the optimization problem to be minimized is given by:

$$f(\boldsymbol{x}) = \sum_{r \in \mathcal{R}} \alpha_r \Delta p_{\mathrm{UFLS},r}(\boldsymbol{x}) \tag{2}$$

where α_r are weighting coefficients; $\Delta p_{\mathrm{UFLS},r}$ are the amount of load shed for the r-th representative contingency; the vector $\boldsymbol{x}$ comprises the decision variables; and $\mathcal{R}$ is the set of representative contingencies identified. In this work, α_r is equal to unity, giving equal weight to all representative contingencies.

A step of the UFLS scheme of island power systems is typically formed by feeders with the same frequency relay settings. Since in smaller island power systems with a limited number of feeders, it will be difficult to find feeder combinations, which finally sum up to the desired step size and respect load priority, the step size (i.e., the amount of load to be shed per step) is not considered as a decision variable in smaller power systems. Thus, the decision variables, which include the parameters of the UFLS scheme and the ESS, are:

- under-frequency (UF) and rate-of-change-of-frequency (RoCoF) thresholds of the UFLS for each shedding step k, namely $\omega_{\mathrm{UF},k}$, $\omega_{\mathrm{RoCoF},k}$, and $\dot{\omega}_k$;
- time delay of the UFLS step k, namely $t_{\mathrm{UF},k}$, $t_{\mathrm{RoCoF},k}$;
- droop and virtual inertia coefficients of the ESS fast-frequency control, namely R_{ESS} and H_{ESS}; and
- tail control coefficient of the ESS, namely $E_{\mathrm{ESS}}^{\mathrm{tail}}$.

Therefore:

$$\boldsymbol{x} = [\boldsymbol{\omega}_{\mathrm{UF}} \ \boldsymbol{\omega}_{\mathrm{RoCoF}} \ \dot{\boldsymbol{\omega}} \ \boldsymbol{t}_{\mathrm{UF}} \ \boldsymbol{t}_{\mathrm{RoCoF}} \ R_{\mathrm{ESS}} \ H_{\mathrm{ESS}} \ E_{\mathrm{ESS}}^{\mathrm{tail}}]^{\mathrm{T}} \tag{3}$$

where $\boldsymbol{\omega}_{\mathrm{UF}}$; $\boldsymbol{\omega}_{\mathrm{RoCoF}}$; $\dot{\boldsymbol{\omega}}$; $\boldsymbol{t}_{\mathrm{UF}}$ and $\boldsymbol{t}_{\mathrm{RoCoF}}$ are vectors containing the under-frequency thresholds of UF and RoCoF relays, the RoCoF thresholds, and time-delay settings for all shedding steps $k \in \mathcal{K}$ of the UFLS scheme.

2) Problem Constraints: The set of constraints of the optimization problem discussed in this section comprises the subset of system constraints, as well as the respective subsets related to the UFLS scheme and the ESS.

The system and UFLS scheme constraints are similar to those proposed in [2] and, for convenience, are recalled below. The system constraints impose the upper and lower admissible bounds for the system frequency, namely $\omega^{\max}$ and $\omega^{\min}$, respectively. Typically, the system frequency is *allowed* to violate such thresholds for a limited amount of time, $t_{\omega^{\max}}$ and $t_{\omega^{\min}}$. Actually, generation units must not trip when frequency falls below $\omega^{\min}$ for a time shorter than $t_{\omega^{\max}}$; therefore, for the r-th representative contingency:

$$\begin{aligned} t_{\omega_r \le \omega^{\min}}(\boldsymbol{x}) &\le t_{\omega^{\min}} \ ; \quad \forall r \in \mathcal{R} \\ t_{\omega_r \ge \omega^{\max}}(\boldsymbol{x}) &\le t_{\omega^{\max}} \ ; \quad \forall r \in \mathcal{R} \end{aligned} \tag{4}$$

The UFLS scheme is further designed such that, for any representative contingency r, no load is shed when the frequency is recovering, i.e., after reaching the frequency nadir at time $t_{nadir,r}$. Moreover, the amount of load shed, $\Delta p_{\mathrm{UFLS},r}$, must not exceed the amount of generation initially lost, $p_{dist,r}$. Thus:

$$\begin{aligned} t_{shed,r}(\boldsymbol{x}) &\le t_{nadir,r}(\boldsymbol{x}) \ ; \quad \forall r \in \mathcal{R} \\ \Delta p_{\mathrm{UFLS},r}(\boldsymbol{x}) &\le p_{dist,r} \ ; \quad \forall r \in \mathcal{R} \end{aligned} \tag{5}$$

Finally, UFLS schemes generally implement the shedding sequence according to a predefined prioritization of the loads. A step k in the prioritized set of steps $\mathcal{K}$ can be implemented only if the previous step $(k-1)$ has already been executed. Thus:

$$\zeta_{r,k}(\boldsymbol{x}) - \zeta_{r,(k-1)}(\boldsymbol{x}) \le 0 \ ; \quad \forall r \in \mathcal{R}, \forall k \in \mathcal{K} \tag{6}$$

where $\zeta_{r,k}(\boldsymbol{x}) \in \{0, 1\}$ is the actuation status of the k-th UFLS step, being 1 if actuated, and 0 otherwise.

Regarding the ESS, a number of constraints need to be included apart from the upper and lower bounds for the power injection and used energy shown in the control scheme of Figure 4. These additional ESS constraints include the upper and lower bounds for the droop, virtual inertia and tail control coefficients, as follows:

$$\begin{aligned} R_{\mathrm{ESS}}^{\min} \le R_{\mathrm{ESS},r} \le R_{\mathrm{ESS}}^{\max} \ ; \quad \forall r \in \mathcal{R} \\ H_{\mathrm{ESS}}^{\min} \le H_{\mathrm{ESS},r} \le H_{\mathrm{ESS}}^{\max} \ ; \quad \forall r \in \mathcal{R} \\ 0 \le E_{\mathrm{ESS},r}^{\mathrm{tail}} \le 100 \ ; \quad \forall r \in \mathcal{R} \end{aligned} \tag{7}$$

Very small values of the inertia or very large values of the droop make the ESS ineffective for primary frequency control, whereas too large inertia values or very small droop values may lead to undesirable dynamic behavior. Common droop values of generators are around 4% and inertia values vary according to the turbine technology between 2 to 5 s in island power systems.

C. Implementation of the Proposed Methodology

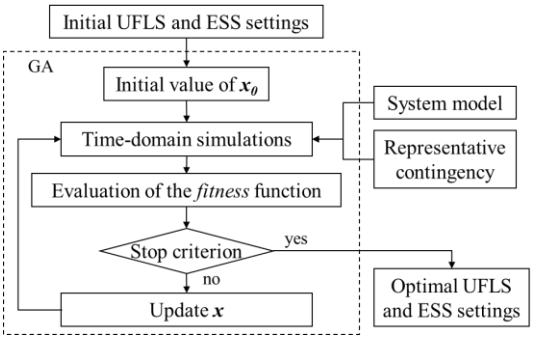

Figure 6. Flow-chart of the proposed methodology to optimize the coordinated control of UFLS scheme and an ESS in island systems.

Given the nonlinear nature of the constraints, the stepped structure of the objective function, and the nonlinearities of the time-domain simulation model, a genetic algorithm (GA) has been applied to solve the optimization problem presented as in [17]. The GA uses a *fitness* function to evaluate a solution $\boldsymbol{x}$, which coincides here with the objective function in equation (2). The interested reader is referred to, e.g., [18]. Figure 6 shows the flow-chart of the proposed methodology to find the optimal settings of the coordinated operation of an UFLS scheme and an ESS in a small island system. Starting from a set of initial values of the decision variables (corresponding typically to the current value of the UFLS and the ESS), the *fitness* function is evaluated by using time-domain simulations considering the model in Figure 1 and the representative contingencies. The values of the decision variables are changed, and the process is repeated, until the criterion to stop the algorithm is met, stage at which the optimal values of the UFLS and ESS parameters have been found.

IV. CASE STUDY

The case study presented in this Section considers the model of a real-world island system that includes an UFLS scheme and an ultracapacitor-based ESS (UC). The objective of this case study is to compare the settings of the UFLS and UC currently implemented in the real-world scenario with the optimal parameters obtained with the proposed coordinated control methodology.

The system description is first provided in Section IV-A. The proposed methodology described in Section III is then applied to optimally design the coordination strategy of the UFLS and UC for a set of four representative contingencies, and results are discussed in Section IV-B. Finally, the proposed methodology is validated in Section IV-C for a set of 164 scenarios combining different contingencies and operating conditions. Section IV-0 compares the optimal coordination with the cases where only either the UFLS or the UC settings are optimized.

A. System Description

The island network, which is part of the Spanish system, comprises 10 diesel and 1 gas generators, and a peak demand of 35 MW. Detailed system data can be found in the Appendix. Table II includes the settings of the steps 1 to 7 of the UFLS scheme used in the real-world system [2]. Finally, the island system includes a 4 MW, 5.6 kWh UC energy storage system, whose features and settings are provided in [15]. The current control parameters have been determined by a trial-and-error process.

The minimum and maximum allowable system frequency values and duration of such violations are:

$$\begin{aligned} \omega^{\min} &= 47 \text{ Hz} \;;\; t_{\omega^{\min}} = 3 \text{ s} \\ \omega^{\max} &= 52 \text{ Hz} \;;\; t_{\omega^{\max}} = 0 \text{ s} \end{aligned} \tag{8}$$

In the remainder of this Section, the following bounds are applied to the decision variables:

$$\begin{aligned} &45 \text{ Hz} \le \omega_{\text{UF},k} \le 50 \text{ Hz} \quad ; \quad \forall k \in \mathcal{K} \\ &49 \text{ Hz} \le \omega_{\text{ROCOF},k} \le 50 \text{ Hz} \; ; \quad \forall k \in \mathcal{K} \\ &-5 \text{ Hz s}^{-1} \le \dot{\omega}_k \le 0 \text{ Hz s}^{-1} \; ; \quad \forall k \in \mathcal{K} \\ &0 \text{ s} \le t_{\text{UF},k} \le 0.5 \text{ s} \quad ; \quad \forall k \in \mathcal{K} \\ &0 \text{ s} \le t_{\text{RoCoF},k} \le 0.5 \text{ s} \quad ; \quad \forall k \in \mathcal{K} \\ &0 \text{ p. u.} \le R_{\text{ESS},r} \le 0.5 \text{ p. u.} \quad ; \quad \forall r \in \mathcal{R} \\ &0 \; s \le H_{\text{ESS},r} \le 20 \text{ s} \quad ; \quad \forall r \in \mathcal{R} \\ &0 \text{ \%} \le E_{\text{ESS},r}^{\text{tail}} \le 100 \text{ \%} \quad ; \quad \forall r \in \mathcal{R} \end{aligned} \tag{9}$$

The time-domain simulations based on the model of Figure 1 and the GA-based optimization were carried out by using Matlab/Simulink. Default function tolerances as suggested in [18] and using a population size of 25 and maximum generation number of 100 have given satisfactory results. RoCoF has been computed by the UFLS block in Figure 1 by approximating the frequency derivative by using time-adjacent frequency values.

B. Optimal Coordination of UFLS and UC for a Subset of Representative Contingencies

In this Section, four representative contingencies have been selected to test the performance of the proposed methodology. Table I shows the contingency scenarios selected according to the system generation and demand consumption conditions, and the loss of generation in MW and in percentage.

TABLE I: REPRESENTATIVE CONTINGENCIES.

Scenario (r)	Generator lost	P_D (MW)	p_{dist} (MW)	p_{dist} (%)
3	G17	18.48	9.55	51.68
10	G20	32.15	6.70	20.84
15	G11	30.74	2.35	7.64
16	G16	29.98	4.74	15.81

The results obtained from applying the proposed methodology to optimize the coordinated UFLS and UC operation are collected in Table II and Table III which compare the current and optimal settings of the UFLS scheme and the UC control, respectively. Note that UFLS steps 1 to 4 in Table II include both underfrequency and RoCoF relays. It can be observed that, with the proposed algorithm, the delays and frequency thresholds of the UFLS steps have been reduced. Moreover, fewer steps are required. Regarding UC settings,

lower values of droop, virtual inertia and, particularly, tail control parameters are obtained from the optimization algorithm.

TABLE II. CURRENT AND OPTIMALLY COORDINATED SETTINGS OF UFLS SCHEME.

Step (k)	$\omega_{UF}/\omega_{ROCOF}$ (Hz)		$\dot{\omega}$ (Hz s^{-1})		t_{UF}/t_{ROCOF} (s)		Step size (%)
	Current	Optimal	Current	Optimal	Current	Optimal	
1	48.81	48.78	-	-	0.3	0.28	6
2	48.81	48.68	-	-	0.6	0.5	0.4
3	48.66	48.43	-	-	1	0.42	10.5
4	48.66	48.03	-	-	1.5	0.25	3.8
5	48.66	-	-	-	2	-	7
6	48	-	-	-	0.8	-	17.4
7	48	-	-	-	1.5	-	8.7
1	49.5	49.56	-1.8	-1.58	0.1	0.1	6
2	49.5	49.51	-1.8	-1.54	0.1	0.08	0.4
3	49.3	49.1	-1.8	-1.56	0.1	0.05	10.5
4	49.3	49.11	-1.8	-1.9	0.1	0.1	3.8

TABLE III. CURRENT AND OPTIMALLY COORDINATED SETTINGS OF THE UC CONTROL.

	R_{ESS} (-)	H_{ESS} (s)	E_{ESS}^{tail} (%)
Current	0.02	10	70
Optimal	0.005	8.9	25

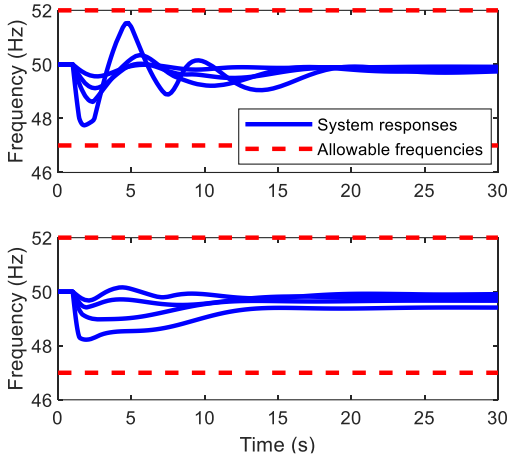

Figure 7. Frequency response of the Spanish island system for the four representative contingencies. Red-dashed horizontal lines indicate ω^{min} and ω^{max}. Top panel: Current UFLS and UC. Bottom panel: Optimal UFLS and UC

Figure 7 shows a comparison of the system responses in terms of frequency to the four representative contingences of Table I. In particular, the impact of the current settings of the UC and UFLS (Current UFLS and UC) is compared with the one of the optimal UFLS and UC settings (Optimal UFLS and UC). Although system responses do not exceed the allowable frequencies threshold ω^{min} in case of the current settings of the UFLS and UC, significant oscillatory behavior can be observed, especially in the case of the most severe contingency (outage of G17 in scenario r = 3). The optimal coordinated operation of the UFLS and UC, shown in the bottom panel of Figure 7, clearly reduces the frequency deviations while also minimizing the oscillatory behavior, thus greatly improving the dynamic performance of the overall system. The relatively small frequency overshoot for scenario r = 15 (see bottom panel in Figure 7) is due to the closed-loop system formed by turbine-governor system action, the UC controls and the equivalent inertia. Figure 8 shows the power injection and energy used of the UC for the most sever contingency. The UC initially injects 4 MW and subsequently reduces its contribution when the frequency starts increasing.

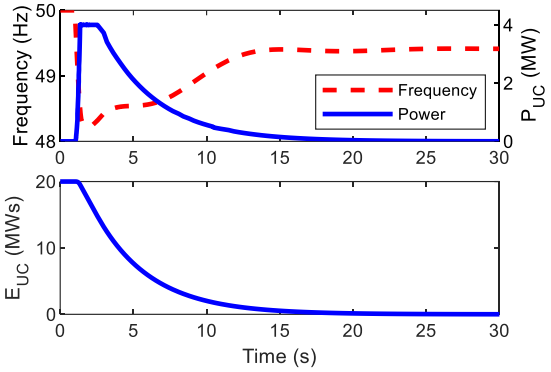

Figure 8. Power injection and energy used of the UC due to the outage of G17 in scenario r = 3 for case (v) - optimal UFLS and UC.

TABLE IV. CUMULATED SHED LOAD AND FREQUENCY VARIATIONS AT FREQUENCY NADIR FOR THE FOUR REPRESENTATIVE CONTINGENCIES.

	Current UFLS and UC	Optimal UFLS and UC
$\sum_{r\in\mathcal{R}} \Delta p_{UFLS}$ (MW)	9.1	3.8
$\sum_{r\in\mathcal{R}} \Delta\omega_{nadir}$ (Hz)	4.9	3.7

Table IV lists the total amount of shed load and frequency variations at frequency nadir, cumulated for the four representative contingencies of Table I. With respect to the current UFLS and UC settings, the total amount of shed load reduces by 60% when the operation of the UFLS and UC is optimally designed with the proposed algorithm. A similar conclusion is drawn for the frequency deviations at the nadir, for which the reduction is 26%. In fact, for scenarios $r = 10, 15, and\ 16$ from Table IV, load shedding actions are not required when optimal coordinated control of UFLS and UC is implemented.

C. Validation of the Optimal Coordination of UFLS and UC for All Contingencies

To come to full circle, this section evaluates the performance of the proposed methodology when simulating a total of 164 different contingencies. Figure 9 shows the system responses in terms of frequency of the Spanish island system facing all 164 contingencies for the cases with Current UFLS and UC (top panel), and Optimal UFLS and UC (bottom panel). It can be observed that the optimal coordination of the UFLS scheme and the UC fast-frequency control leads to a reduction of the overall frequency deviations, keeping the system frequency always within its thresholds and, simultaneously, to a significant damping of the oscillations due to, e.g., UC full-discharge events. The simulations of the 164

contingencies confirm the results obtained when considering the representative contingencies.

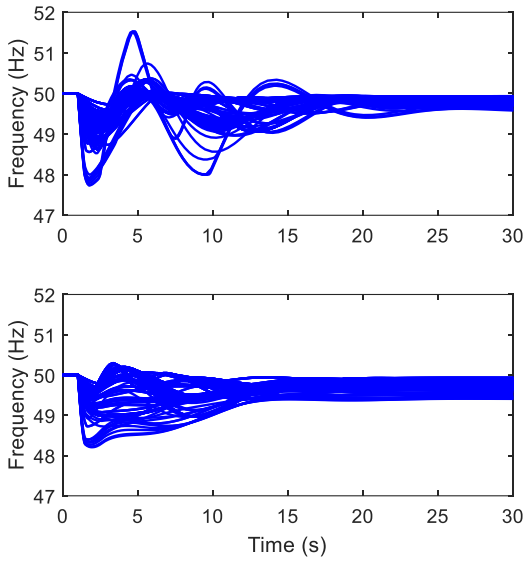

Figure 9. Frequency response of the Spanish island system for the 164 contingencies. Top panel: Current UFLS and UC. Bottom panel: Optimal UFLS and UC.

Table V lists the total amount of load shed and frequency variations at frequency nadir, cumulated for the 164 contingencies simulated. Comparing the current UFLS and UC settings with the optimal UFLS and UC settings shows that the amount of load shed and frequency nadir variations are reduced by around 64% and 22%, respectively.

TABLE V. CUMULATED SHED LOAD AND FREQUENCY VARIATIONS AT FREQUENCY NADIR FOR ALL 164 REPRESENTATIVE CONTINGENCIES.

	Current UFLS and UC	Optimal UFLS and UC	Optimal UFLS and Current UC	Current UFLS and Optimal UC
$\sum_{r\in\mathcal{R}} \Delta p_{\text{UFLS}}$ (MW)	134.7	48.5	99.1	66.2
$\sum_{r\in\mathcal{R}} \Delta\omega_{nadir}$ (Hz)	142.4	111.6	141.9	111.8

Finally, the methodology described in reference [2] has been applied but without UC. The simulation of the 164 contingencies with the resulting optimized UFLS scheme only leads to a total amount of load shed and frequency variations at frequency nadir of 181.95 MW and 213.26 Hz, respectively. Worse results with respect to the amount of shed load and frequency variations justify the installation of the UC.

D. Sensitivity Analysis

This section compares the optimal coordinated operation of the UFLS and UC with the cases for which only either the UFLS (Optimal UFLS and Current UC) or the UC settings (Current UFLS and Optimal UC) are optimized. For this purpose, the decision variables related to the UC or to the UFLS of eq. (3) are respectively omitted.

Figure 10 shows the system responses in terms of frequency of the Spanish island system facing all 164 contingencies for the cases with Optimal UFLS and Current UC (top panel), and Current UFLS and Optimal UC (bottom panel). When comparing Figure 9 and Figure 10, it can be observed that optimizing only the UFLS settings leads to a reduction of the frequency overshoots after the first swing, but the frequency nadir does not significantly improve with respect to the current UFLS and UC settings. Optimizing the UC settings, on the other hand, both under- and over-frequency deviations are greatly reduced. However, the oscillatory behavior remains to some extent.

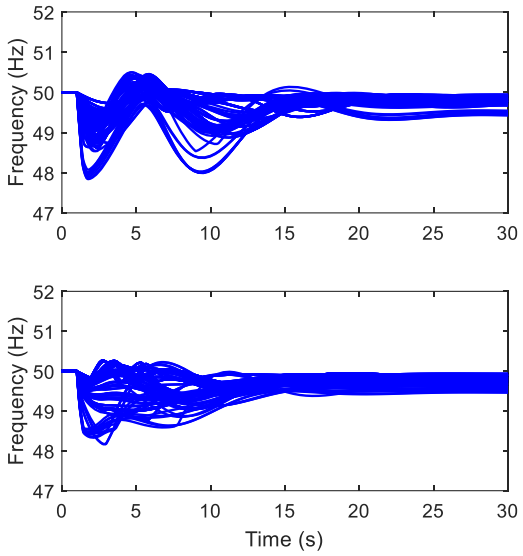

Figure 10. Frequency response of the Spanish island system for the 164 contingencies. Top panel: Optimal UFLS and Current UC. Bottom panel: Current UFLS and Optimal UC.

Table V also quantifies total amount of load shed and frequency variations at frequency nadir for the optimized UFLS and current UC settings and for the current UFLS and optimal UC settings. It can be seen that the best results in terms of total amount of shed load are obtained when the operation of the UFLS scheme and UC controller are optimally coordinated using the proposed methodology. In terms of frequency variations at frequency nadir, the optimal UFLS and UC settings lead to similar results than the optimal UC and current UFLS settings but with the benefit of using a smaller amount of shed load mainly due to the lower underfrequency threshold settings of UFLS steps 1 to 4. Another interesting result from Table V is that optimizing only the UC control parameters shows significantly better performance than optimizing only the UFLS scheme settings. This is partially due to the fact that the step size has not been considered as a decision variable for smaller power systems, limiting the effect of varying the other parameters of the UFLS scheme.

V. CONCLUSIONS

In this paper, a methodology to optimally coordinate the joint operation of under-frequency load shedding (UFLS)

schemes and fast-responding, converter-interfaced energy storage systems (ESS) to mitigate under-frequency events in island power systems has been proposed. In particular, the optimization algorithm determines the optimal set of parameters of the UFLS relay settings and the ESS fast-frequency controllers that minimize the number of load shedding actions.

Simulation results from a real-world Spanish island system with UFLS schemes and an ultracapacitor (UC)-based ESS show a significant improvement of the system overall performance when the proposed methodology is applied compared with the currently implemented settings of the UFLS and UC. Moreover, the proposed approach outperforms the individual optimal design of the UFLS or the UC.

Future work will focus on the coordination of UFLS and several ESSs of different technologies. The work can be also extended to coordinate the settings of the frequency controller of renewable energy resources under deloaded operation, offering a limited amount of energy available to provide primary frequency control support, to include the step size of UFLS schemes. Finally, reliability of UC modules will be considered.

VI. ACKNOWLEDGMENT

This study is funded by European Regional Development Fund (ERDF), Ministerio de Ciencia e Innovación - Agencia Estatal de Investigación, Project RTI2018-100965-A-I00.

VII. APPENDIX

TABLE VI. GENERATOR DATA OF THE SPANISH ISOLATED SYSTEM

	G11	G12	G13	G14	G15	G16	G17	G18	G19	G20	G21
H (s)	1.75	1.75	1.75	1.73	2.16	1.88	2.1	6.5	2.1	2.1	2.1
c (pu)	20	20	20	20	20	20	20	21.5	20	20	20
b_1 (s)	1.44	1.44	1.44	1.44	1.32	1.43	1.32	0.89	1.32	1.32	1.32
b_2 (s)	0	0	0	0	0	0	0	0	0	0	0
a_1 (s)	18.64	18.64	18.64	18.64	18.38	18.66	18.31	5.66	18.31	18.31	18.31
a_2 (s)	3.98	3.98	3.98	3.98	2.7	3.85	2.71	3.48	2.71	2.71	2.71
$p^{\min}$ (MW)	2.5	2.5	2.5	3	3.5	3.5	7	0	7	7	7
$p^{\max}$ (MW)	4	4	4	4.5	7	7	12	22.8	12	12	12
M_{base} (MVA)	5.4	5.4	5.4	6.3	9.4	9.6	15.75	26.82	14.5	14.5	14.5

TABLE VII. SCENARIOS OF GENERATION OPERATING CONDITIONS

Scenario	G11	G12	G13	G14	G15	G16	G17	G18	G19	G20	G21	Total
1	2.35	0	2.35	0	3.29	3.69	10.41	0	0	0	0	22.09
2	0	0	2.35	0	3.29	4.26	9.26	0	0	0	0	19.16
3	0	0	2.35	0	3.29	3.29	9.55	0	0	0	0	18.48
4	0	0	2.35	0	3.29	3.69	8.96	0	0	0	0	18.29
5	0	0	2.35	0	3.29	3.29	9.35	0	0	0	0	18.28
6	0	0	2.35	0	3.29	3.29	9.61	0	0	0	0	18.54
7	2.35	0	2.35	0	3.29	3.29	10.02	0	0	0	0	21.30
8	2.53	0	2.53	0	5.84	5.84	0	0	6.63	4	0	27.37
9	2.35	0	2.35	2.82	4.92	4.92	0	0	6.63	6.7	0	30.69
10	2.41	0	2.41	2.82	5.59	5.59	0	0	6.63	6.7	0	32.15
11	2.46	0	2.46	2.82	5.69	5.69	0	0	6.63	6.7	0	32.45
12	2.49	0	2.49	2.82	5.77	5.77	0	0	6.63	6.7	0	32.67
13	2.58	0	2.58	2.82	5.96	5.96	0	0	6.63	6.7	0	33.23
14	2.4	0	2.4	2.82	5.56	5.56	0	0	6.63	6.7	0	32.07
15	2.35	2.35	2.35	2.82	5.12	5.12	0	0	6.63	4	0	30.74
16	2.35	2.35	2.35	2.82	4.74	4.74	0	0	6.63	4	0	29.98
17	2.35	2.35	2.35	2.82	4.22	4.22	0	0	6.63	4	0	28.94
18	2.35	2.35	2.35	0	3.29	3.29	9.21	0	6.63	0	0	29.47
19	2.35	2.35	2.35	0	3.29	3.29	8.68	0	6.63	0	0	28.94
20	2.35	2.35	2.35	0	3.29	3.29	9.35	0	6.63	0	0	29.61
21	2.35	2.35	2.35	0	3.71	3.71	11.38	0	6.63	0	0	32.48
22	2.35	2.35	2.35	0	3.58	3.58	11.38	4.85	6.63	0	0	37.07
23	2.35	2.35	2.35	0	3.63	3.63	11.38	0	6.63	0	0	32.32
24	2.35	2.35	2.35	0	3.29	3.29	6.63	0	6.63	0	0	26.89
25	0	0	2.35	0	3.29	3.29	9.16	0	0	0	0	18.09
26	2.35	2.35	2.35	0	3.58	3.58	11.38	4.85	6.66	0	0	37.10

VIII. REFERENCES

[1] D. Ochoa and S. Martinez, "Modeling an Isolated Hybrid Wind-Diesel Power System for Performing Frequency Control Studies. A Case of Study: San Cristobal Island, Galapagos-Ecuador," *IEEE Lating America Transactions*, vol. 17, no. 5, pp. 775-787, 2019.

[2] L. Sigrist, I. Egido and L. Rouco, "A Method for the Design of UFLS Schemes of Small Isolated Power Systems," *IEEE Transactions on Power Systems*, vol. 27, no. 2, pp. 951-958, 2012.

[3] P. M. Anderson, Power System Protection, Piscataway, NJ (USA): IEEE Press, 1999, pp. 1249-1258.

[4] U. Akram, M. Nadarajah, R. Shah and F. Milano, "A Review on Rapid Responsive Energy Storage Technologies for Frequency Regulation in Modern Power Systems," *Renewable and Sustainable Energy Reviews*, vol. 120, 2020.

[5] S. Koohi-Kamali and N. A. Rahim, "Coordinated Control of Smart Microgrid During and After Islanding Operation to Prevent Under Frequency Load Shedding Using Energy Storage System," *Energy Conversion and Management*, vol. 127, pp. 623-646, 2016.

[6] S. Pulendran and J. E. Tate, "Energy Storage System Control for Prevention of Transient Under-Frequency Load Shedding," *IEEE Transactions on Smart Grid*, vol. 8, no. 2, pp. 927-936, 2017.

[7] S. Chandak, P. Bhowmik and P. K. Rout, "Robust Power Balancing Scheme for the Grid-Forming Microgrid," *IET Renewable Power Generation*, vol. 14, no. 1, pp. 154-163, 2020.

[8] L. Sigrist, L. Rouco and C. Jiménez Serrano, "Sizing of a Battery Energy Storage System to Minimize Underfrecuency Load Shedding in Island Power Systems," in *25th International Conference and Exhibition on Electricity Distribution - CIRED 2019*, Madrid, 2019.

[9] J. Cao, W. Du, H. Wang and M. McCulloch, "Optimal Sizing and Control Strategies for Hybrid Storage System as Limited by Grid Frequency Deviations," *IEEE Transactions on Power Systems*, vol. 33, no. 5, pp. 5486-5495, 2018.

[10] S. You, Y. Liu, J. Tan, M. T. Gonzalez, X. Zhang, Y. Zhang and Y. Liu, "Comparative Assessment of Tactics to Improve Primary Frequency Response Without Curtailing Solar Output in High Photovoltaic Interconnection Grids," *IEEE Transactions on Sustainable Energy*, vol. 10, no. 2, pp. 718-728, 2019.

[11] A. Rafinia, J. Moshtagh and N. Rezaei, "Stochastic optimal robust design of a new multi-stage under-frequency load shedding system considering renewable energy sources," *International Journal of Electrical Power & Energy Systems*, vol. 118, no. 105735, 2020.

[12] M. N. Acosta, C. Adiyabazar, F. Gonzalez-Longatt, M. A. Andrade, J. R. Torres, E. Vazquez and J. M. R. Santos, "Optimal Under-Frequency Load Shedding Setting at Altai-Uliastai Regional Power System, Mongolia," *Energies*, vol. 13, no. 20, p. 5390, 2020.

[13] S. S. Banijamali and T. Amraee, "Semi-Adaptive Setting of Under Frequency Load Shedding Relays Considering Credible Generation Outage Scenarios," *IEEE Transactions on Power Delivery*, vol. 34, no. 3, pp. 1098-1108, 2018.

[14] P. Kundur, Power System Stability and Control, New York: McGraw-Hill, 1994.

[15] I. Egido, L. Sigrist, E. Lobato, L. Rouco and A. Barrado, "An Ultra-Capacitor for Frequency Stability Enhancement in Small-Isolated Power Systems: Models, Simulation and Field Tests," *Applied Energy*, vol. 137, pp. 670-676, 2015.

[16] J. Abonyi and B. Feil, Cluster Analysis for Data Mining and System Identification, Basel: Birkhäuser, 2007.

[17] J. A. P. Lopes, M. A. Mitchell and e. al., "Optimum Determination of Underfrequency Load Shedding Strategies Using a Genetic Algorithm Approach," in *Proceedings of the Thirty-Second Annual North American Power Symposium*, Waterloo, Ont. (Canada), 2000.

[18] The MathWorks, "Genetic Algorithm and Direct Search Toolbox User's Guide," 2004.